NASA/TM–2005-212831

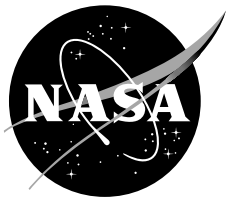

Techniques for Transition and Surface Temperature Measurements on Projectiles at Hypersonic Velocities—A Status Report

D. W. Bogdanoff
ELORET, Sunnyvale, California

M. C. Wilder
Ames Research Center, Moffett Field, California

July 2005

The NASA STI Program Office . . . in Profile

Since its founding, NASA has been dedicated to the advancement of aeronautics and space science. The NASA Scientific and Technical Information (STI) Program Office plays a key part in helping NASA maintain this important role.

The NASA STI Program Office is operated by Langley Research Center, the Lead Center for NASA's scientific and technical information. The NASA STI Program Office provides access to the NASA STI Database, the largest collection of aeronautical and space science STI in the world. The Program Office is also NASA's institutional mechanism for disseminating the results of its research and development activities. These results are published by NASA in the NASA STI Report Series, which includes the following report types:

- TECHNICAL PUBLICATION. Reports of completed research or a major significant phase of research that present the results of NASA programs and include extensive data or theoretical analysis. Includes compilations of significant scientific and technical data and information deemed to be of continuing reference value. NASA's counterpart of peer-reviewed formal professional papers but has less stringent limitations on manuscript length and extent of graphic presentations.

- TECHNICAL MEMORANDUM. Scientific and technical findings that are preliminary or of specialized interest, e.g., quick release reports, working papers, and bibliographies that contain minimal annotation. Does not contain extensive analysis.

- CONTRACTOR REPORT. Scientific and technical findings by NASA-sponsored contractors and grantees.

- CONFERENCE PUBLICATION. Collected papers from scientific and technical conferences, symposia, seminars, or other meetings sponsored or cosponsored by NASA.

- SPECIAL PUBLICATION. Scientific, technical, or historical information from NASA programs, projects, and missions, often concerned with subjects having substantial public interest.

- TECHNICAL TRANSLATION. English-language translations of foreign scientific and technical material pertinent to NASA's mission.

Specialized services that complement the STI Program Office's diverse offerings include creating custom thesauri, building customized databases, organizing and publishing research results . . . even providing videos.

For more information about the NASA STI Program Office, see the following:

- Access the NASA STI Program Home Page at *http://www.sti.nasa.gov*

- E-mail your question via the Internet to help@sti.nasa.gov

- Fax your question to the NASA Access Help Desk at (301) 621-0134

- Telephone the NASA Access Help Desk at (301) 621-0390

- Write to:
  NASA Access Help Desk
  NASA Center for AeroSpace Information
  7121 Standard Drive
  Hanover, MD 21076-1320

NASA/TM–2005-212831

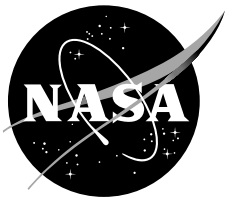

Techniques for Transition and Surface Temperature Measurements on Projectiles at Hypersonic Velocities—A Status Report

D. W. Bogdanoff
ELORET, Sunnyvale, California

M. C. Wilder
Ames Research Center, Moffett Field, California

National Aeronautics and
Space Administration

Ames Research Center
Moffett Field, California 94035-1000

July 2005

Acknowledgments

The delicate fabrication work of projectiles was performed with great skill by L. M. Ford, C. A. Stangeland, and R. T. Piquette. The projectiles were launched and the shadowgraphs and time data were taken by the gunners D. M. Holt, D. B. Bowling, R. E. Smythe, and R. Stewart, and ballistic range manager C. J. Cornelison. Their work is outstanding. A number of very valuable suggestions that helped us to solve problems of projectile integrity, unacceptably large pitch and yaw angles, and graphite surface quality were made by the machinists, the gunners, and the range manager. D. C. Reda was the project leader and offered many valuable suggestions that contributed to the success of the project. Support by NASA (Contract NAS-2-99092) to Eloret is gratefully acknowledged.

TABLE OF CONTENTS

TECHNIQUES FOR TRANSITION AND SURFACE TEMPERATURE MEASUREMENTS ON PROJECTILES AT HYPERSONIC VELOCITIES—A STATUS REPORT

D. W. Bogdanoff* and M. C. Wilder‡

Ames Research Center

SUMMARY

A research effort to advance techniques for determining transition location and measuring surface temperatures on graphite-tipped projectiles in hypersonic flight in a ballistic range is described. Projectiles were launched at muzzle velocities of ~4.7 km/sec into air at pressures of 190–570 Torr. Most launches had maximum pitch and yaw angles of 2.5–5 degrees at pressures of 380 Torr and above and 3–6 degrees at pressures of 190–380 Torr. Arcjet-ablated and machined, bead-blasted projectiles were launched; special cleaning techniques had to be developed for the latter class of projectiles. Improved methods of using helium to remove the radiating gas cap around the projectiles at the locations where ICCD (intensified charge coupled device) camera images were taken are described. Two ICCD cameras with a wavelength sensitivity range of 480–870 nm have been used in this program for several years to obtain images. In the last year, a third camera, with a wavelength sensitivity range of 1.5–5 microns [in the infrared (IR)], has been added. ICCD and IR camera images of hemisphere nose and 70-degree sphere-cone nose projectiles at velocities of 4.0–4.7 km/sec are presented. The ICCD images clearly show a region of steep temperature rise indicative of transition from laminar to turbulent flow. Preliminary temperature data for the graphite projectile noses are presented.

* Senior Research Scientist, Eloret, Sunnyvale, CA 94087.

‡ Aerospace Engineer, NASA Ames Research Center, CA 94035.

I. INTRODUCTION

Modelling of roughness-dominated transition is a critical design issue for thermal protection systems (TPS). Ablating TPS, for single-use planetary-entry and earth-return missions, first experience recession under high-altitude, low-Reynolds-number conditions. Such laminar-flow ablation causes the formation of a distributed surface-microroughness pattern characteristic of the TPS material's composition and fabrication process. These roughness patterns create disturbances within the laminar boundary layer flowing over the surface. As altitude decreases, Reynolds number increases and flowfield conditions capable of amplifying these roughness-induced perturbations are eventually achieved and transition to turbulent flow occurs. Boundary-layer transition to turbulence results in higher heat transfer and ablation rates (refs. 1, 2).

In order to better understand this process, ballistic-range nosetip-transition experiments were carried out in the 1970s. Three bulk graphite and two carbon/carbon composite nosetip materials were studied (refs. 2–7). Nosetips were ablated before launch in a low-pressure, high-enthalpy, arcjet environment to create the proper initial condition (characteristic microroughness) for each material. For each material tested, at least one nosetip was sectioned and the microroughness distribution determined by microscopy. All remaining nosetips were mounted on ballistic-range models and launched at velocities of 3.5–5.0 km/sec into a well-defined clean air environment. With the exception of three shots with ATJ-S graphite models, all tests were conducted on the G track range at the Arnold Engineering and Development Center (AEDC) (ref. 8).

Nosetip surface-temperature contours were measured for each shot using cameras sensitive to visible and near infrared radiation. This technique allowed the determination of the transition-front contour and the mean transition-front location. Measurements of nosetip surface roughness, surface temperature, average transition-front location, and the freestream environment were combined with results of calculations of laminar boundary-layer development in nosetip flowfields to transform the data into various non-dimensional parameters. These parameters were established by earlier attempts to correlate existing wind tunnel data for transition on rough/blunt bodies. Only one of the earlier correlation methods was found to successfully describe the wind-tunnel and ballistic-range data. Further details are given in references 9–13.

In addition to measuring the position of the transition front, quantitative heat-flux information can be obtained from surface temperature measurements. The heat-flux data can be obtained from the nosetip surface temperature data by solving the unsteady one-dimensional heat conduction equation in the carbon-carbon or graphite nosetip. Accurate heat-flux measurements can be used to establish heat-transfer correlations for laminar and turbulent flow. The correlations then can be used to validate CFD codes used for entry-vehicle design.

An effort was started in 2001, at the NASA Ames Research Center (ARC), to implement and further develop these earlier ballistic-range transition and heat-transfer measurement techniques to support current and future earth and planetary entry studies. New TPS materials, such as the diborides (ZrB_2 and HfB_2), could be studied along with new shape concepts, such as swept-back leading edges. Also, studies could be carried out in gases other than air, such as those that are typical of the atmospheres of Mars and Titan. Further, using new-technology cameras (refs. 14, 15), surface temperature

measurements down to 400 K could be measured, which was not possible during the studies of the 1970s. The ARC program started with validation of the experimental technique, i.e., reproduction of the results of the 1970s work discussed above. The first part of this effort was reported in references 16 and 17. These references discussed range and gun operating conditions, the design of hemisphere-nose and 70-degree sphere-cone graphite-tipped projectiles, pitch and yaw angles and oscillation wavelengths of the projectiles, and the use of helium plumes to remove the glowing gas cap in front of the projectile. Projectile images obtained in the Ames Aerodynamics Range showing transition fronts were presented in references 16 and 17.

The present report describes the continuation of the previous work. Section II discusses operation of the range and the gun operating conditions. Section III presents projectile designs for hemisphere-nose and 70-degree sphere-cone projectiles. With a new projectile design for the latter class of projectiles, consistent satisfactory launches are now being obtained. Section IV presents data on the pitch and yaw angles, oscillation wavelengths, and swerves for the hemisphere-nose and 70-degree sphere-cone projectiles. (Swerves are the distances of the projectile from the range centerline.) The present report presents substantially larger data sets than did previous reports. Section V discusses the use of helium in the range to remove the radiation from the hot gas cap covering the projectile nose. A new, proven technique is reported. A new method for minimizing the loss of graphite dust from the projectile nose is also discussed in this section. In the same section, the wavelength sensitivities of the cameras used to photograph the projectiles are given and calibration techniques for the cameras are described. Use of a new IR (3–5- micron) camera is described. Section VI presents photographs showing the transition fronts and preliminary surface temperature data.

II. OPERATION OF RANGE AND GUN OPERATING CONDITIONS

The projectiles launched at AEDC, with only three exceptions, were fired in a track range—that is, after exiting the gun muzzle, the projectiles flew along a system of four rails that maintained the projectile attitude. Free-flying projectiles were used for the present study. These projectiles must be aerodynamically stable, and it is desirable to have maximum pitch and yaw angles of 5–6 degrees or less. Larger pitch and yaw angles would mean that observed projectile surface temperature variations would correspond to averaging over too great a variation of projectile heat fluxes to provide good correlations. Much of the earlier work at AEDC was done with a launcher bore diameter of 6.35 cm. The present program was carried out using the largest two-stage gun available at ARC, with a bore diameter of 3.81 cm. To obtain the largest possible projectile diameters and to minimize projectile pitch and yaw angles, we decided to use bore-rider projectiles rather than sabot-launched projectiles. Figure 1 shows a sketch of the Ames Aerodynamics Range, showing the gun, muzzle-blast dump tank, sabot stripper (not necessary for the present projectiles), the range proper with 16 orthogonal shadowgraph stations, and the catch butt. Two ICCD cameras take nearly head-on images of the projectile, using mirrors as shown in the figure. The IR camera images the projectile at station 3 using a mirror in the same manner as shown for the ICCD cameras.

Representative launch conditions for our graphite-nose projectiles were as follows:

Ames 3.81-cm/15.88-cm light gas gun.
Pump tube volume: 426,000 cm^3
Powder type: IMR/Dupont 4227—booster charge (200 grams);
Hercules HC-33-FS—main charge
Powder mass (total): 2200–2300 grams
Piston mass: 21.3 kg
Piston material: high-density polyethylene
Piston velocity: 557–588 m/sec
Hydrogen pressure: 4.71 bar
Break-valve rupture pressure: 172–241 bar
Projectile mass: 96–115 grams
Muzzle velocity: 4.6–5.1 km/sec

III. PROJECTILE DESIGNS

Cross-sections of projectiles that were launched in the present program are shown in figure 2. (We will refer herein to the plastic, cylindrical bore-riding part of the projectile as the "afterbody.") This type of design avoids the asymmetrical disturbance to the projectile, which occurs upon sabot separation. These projectiles are short and heavily weighted forward with steel and tungsten to provide aerodynamic stability. This type of design is necessary, because the cylindrical portion of the projectile provides very little aerodynamic restoring moment and the center of pressure is only about half a projectile diameter aft of the center of the projectile nose. The projectiles must also be stable against tilt upon launch down the barrel. This stability was maintained by setting the minimum allowable bore-riding length of the projectile to 0.83 times the barrel diameter. This ratio was based on extensive experience in the Ames ballistic ranges.

POCO FM-1 graphite is used for the projectile noses. The graphite noses are bonded to the steel and tungsten of the projectile using TRA-CON 2112 epoxy. An epoxy thickness of 0.13 mm is maintained by using a mixture of epoxy and 0.13-diameter glass spheres for the bond joint. After applying the epoxy to the joint, a weight of ~2.3 kg is applied to the graphite, which is held in an aluminum fixture, to assure uniform distribution of the epoxy and expulsion of excess epoxy. The tungsten weight in the projectile is made of a machinable tungsten alloy, Kulite K1700.

The epoxy-filled holes shown in figure 2 provide brilliant fiducial points in the head-on ICCD camera images taken of the projectile. Some earlier projectile designs (ref. 16) had graphite pins instead of epoxy-filled holes. The epoxy-filled holes were found to be just as effective and considerably easier to fabricate. For the latest projectile design (as of April, 2004—see fig. 2c), shallow holes without epoxy filling were used. These were still easier to fabricate and were also found to be very effective as fiducial markers. To allow for determination of projectile roll, some

projectiles used in later experiments used 7 holes on an 8-hole pattern (i.e., one hole of the pattern is missing). Roll rates were found to be very small, so we have returned to an 8-hole pattern for the latest projectiles.

Fourteen hemisphere nose projectiles and eight 70-degree sphere-cones have been successfully launched in the Ames Aerodynamics Range. The graphite noses for 8 hemisphere-nose projectiles were pre-ablated in one of the Ames arcjets under laminar flow conditions for various lengths of time, producing varying degrees of surface recession. The characteristic surface roughness was quantified by sectioning one model (not launched in the range) and measuring its roughness under a microscope. The mean surface roughness was 17 microns peak-to-valley. Most of the remaining projectiles were bead-blasted in the shop to provide a controlled roughness. Some difficulty was found with the bead-blasted projectiles in that apparently graphite dust was being released from the projectiles as they flew down the range, tending to obscure the surface images. A special cleaning technique developed to deal with this problem is described in Section V.

Bore-rider projectiles with afterbodies made of polyethylene, high-impact ABS (acrylonitrile-butadiene-styrene) and Zytel ST-801 Nylon were launched. [Lexan (polycarbonate) was considered, but because the greater density of Lexan makes it difficult to have the center of gravity of the projectile sufficiently far forward to achieve adequate aerodynamic stability, it was rejected.] The ABS was found to have adequate mechanical properties, but it smoked and burned sufficiently strongly to severely obscure the ICCD camera images taken to determine transition location and surface temperature. Polyethylene was found to be too weak, deforming under the launch loads. Nylon produced the least smoking and burning of the three plastics tested. Hence, Nylon was the material of choice for the projectile afterbodies.

The mechanical properties of the Zytel ST-801 Nylon given in reference 18 are excellent for the present test program, with a tensile strength of 6000 psi and an Izod impact strength of 20 ft-lbf/in. A number of successful shots had already been made with this Nylon when, in shot 2307, the projectile afterbody disintegrated. Izod impact tests of a new rod of Nylon indicated mean impact strengths of 2.6 ft-lbf/in, only 13% of the value quoted in the manufacturer's brochure for injection-molded Nylon. Two more rods of Nylon were obtained and Izod specimens fabricated and tested, yielding impact strengths from 6.5 to 15 ft-lbf/in. Projectiles made from the latter two rods were successfully launched. We concluded that Zytel ST-801 Nylon was the best material for the projectile afterbodies, but one must verify that the impact strength of each rod purchased is satisfactory before fabricating and launching projectiles. Further discussion of the plastics used for the projectile afterbodies was given in references 16 and 17.

In addition to the material properties issue discussed above, two difficulties were found in the first design of the 70-degree sphere-cone projectile shown in figure 2b. The afterbody of one of these projectiles disintegrated upon launch, even though the Izod impact strength of the Nylon used for the afterbody had been determined to be satisfactorily high. It is believed that the most likely cause of the problem was insufficient distance between the aftmost end of the main steel nosepiece and the aft end of the projectile proper. During compression of the hydrogen gas in the pump tube of the two-stage gas gun launcher, strong shock waves strike the aft end of the projectile. It is believed that these shock waves reflect from the aftmost steel surface in the projectile and that if these waves are not sufficiently attenuated by distance before striking the aft end of the projectile, they can reflect

there as rarefaction waves and exceed the tensile strength of the projectile, causing the projectile afterbody to fail. By lengthening the plastic projectile afterbody 0.45 cm, this problem was solved. However, a second problem occurred upon launching the lengthened version of the projectile shown in figure 2b. The plastic afterbody of this design includes a long, thin annular region outside the steel at the front end of the projectile. Part of this annular region separated from the projectile during the launch. In the design of version 2, shown in figure 2c, this annular plastic region is shortened and is partially restrained by the main steel nosepiece. This design change eliminated the second problem. With the latest projectile designs, shown in figures 2a and 2c, successful launches have been obtained for the last 14 shots (shots 2319–2332).

IV. PROJECTILE DYNAMICS

Because our projectiles are flying free, the maximum pitch and yaw angles must be maintained within reasonably small limits. In general, in the region just beyond the muzzle, the projectile will receive a torque-time impulse due to non-axisymmetric expansion of the muzzle-blast gas. The projectile will then exit the muzzle-blast region with the pitch and yaw angles increasing at certain rates produced by the torque-time impulse. Assuming that the projectile is statically stable, after it leaves the muzzle region with the given pitch rate, it will execute an approximately sinusoidal motion in pitch angle (ignoring pitch damping) due to aerodynamic restoring forces. The maximum pitch angle reached can be shown to vary linearly with the initial pitch rate and the wavelength of the oscillation (ref. 16). Hence, the maximum pitch angle can be reduced by either reducing the torque-time impulse at the muzzle (i.e., reducing the initial pitch rate) or by increasing the aerodynamic restoring force, which shortens the wavelength of the pitch oscillation. (All arguments presented here apply equally to pitch and yaw oscillations, so, for brevity, only pitch oscillations are discussed in what follows.) In general, to increase the aerodynamic restoring force, we have simply designed the projectile to place the center of gravity as far forward as possible, consistent with adequate projectile strength. Steps taken to reduce disturbances at the muzzle are described in reference 16.

Maximum pitch and yaw angles (with respect to the range axis) for 23 successful shots are given in table 1. The table contains data for 14 graphite hemisphere shots, eight 70-degree graphite sphere-cone shots, and one copper hemisphere shot. For a given projectile and given initial pitch or yaw rates at the muzzle, simple theoretical analyses (ref. 16) predict that both the maximum pitch and yaw angles and the wavelengths of the pitch and yaw oscillations vary as the range pressure to the –0.5 power. For the projectiles for which data are shown in table 1, figure 3 shows the maximum absolute pitch or yaw angle (whichever is greater) plotted versus the range pressure. Figure 4 shows, for the same projectiles, the oscillation wavelength versus the range pressure. These data were obtained by reading the shadowgraphs taken for each shot. [Different pressure ranges were used for the two classes of projectiles because the location of the transition region (at a given range pressure) was very different for the two different projectile nose shapes.]

Table 1. Maximum pitch and yaw angles.

Shot Number	Type of Model	Range Pressure (Torr)	Maximum Pitch Angle (Degrees)	Maximum Yaw Angle (Degrees)
2306	Graphite hemisphere	380	4.8	4.6
2309	Graphite hemisphere	380	1.6	3.0
2310	Graphite hemisphere	380	1.7	3.0
2311	Graphite hemisphere	190	1.6	3.5
2312	Graphite hemisphere	285	2.4	3.4
2313	Graphite hemisphere	198	0.8	2.1
2314	Graphite hemisphere	101	2.9	12.6
2315	Graphite hemisphere	241	3.6	5.3
2316	Graphite hemisphere	162	8.1	4.3
2319	Gr. 70-deg. sph.-cone	380	5.0	3.5
2320	Gr. 70-deg. sph.-cone	570	3.4	2.5
2321	Gr. 70-deg. sph.-cone	570	4.5	6.2
2322	Gr. 70-deg. sph.-cone	382	9.5	3.9
2323	Graphite hemisphere	287	3.7	1.9
2324	Graphite hemisphere	191	7.8	3.5
2325	Graphite hemisphere	190	2.7	3.5
2326	Graphite hemisphere	191	5.7	4.9
2327	Copper hemisphere	381	12.8	11.0
2328	Graphite hemisphere	190	4.0	5.9
2329	Gr. 70-deg. sph.-cone	571	2.6	1.7
2330	Gr. 70-deg. sph.-cone	500	2.5	1.5
2331	Gr. 70-deg. sph.-cone	440	2.6	3.0
2332	Gr. 70-deg. sph.-cone	440	2.0	4.5

In figure 3, the maximum angles observed are divided into "good," "acceptable," and "not acceptable" ranges, as indicated near the ordinate axis. Only data in the first two catagories were used for further transition and surface temperature studies. Pitch and yaw angles in the "not acceptable" range (> 6 degrees) would mean that observed projectile surface-temperature variations would correspond to averaging over too great a variation of projectile heat fluxes to provide good correlations. A six-degree maximum pitch or yaw angle corresponds to a peak-to-peak motion of the heat flux pattern of ~0.40 cm on the projectile nose. For comparison, the projectile diameter and the equivalent sphere diameter of the hemisphere-nose projectile are 3.81 cm. Reference 19 gives plots of heat flux versus angle from the stagnation point for hypersonic flow over a hemisphere. From these plots, the percentage peak-to-peak variations of heat transfer for a peak-to-peak angular motion of 12 degrees (corresponding to a six-degree maximum pitch or yaw angle) are 8%, 15%, and 23% for angles from the stagnation point of 20, 30, and 40 degrees, respectively. The changes in the average heat transfer rates due to the angular motion are much less, about 2%. These variations were judged to be acceptable.

Figure 3 also shows two least-square power law curve fits. The first fit is a two-parameter fit of the form (maximum pitch angle) or (oscillation wavelength) = A (range pressure)^{B}. The exponent is

determined by the fit. The second fit is of the form (maximum pitch angle) or (oscillation wavelength) = A (range pressure)$^{-0.5}$, i.e., the theoretical exponent is used. Figure 4 shows four least-square power law fits, two with the theoretical exponent of -0.5 and two with free exponents.

In figure 3, the two 70-degree sphere-cone data points with the highest maximum angles were from two successive shots (shots 2321 and 2322) where there was some doubt that the rupture diaphragm of the two-stage gun had been correctly installed. After these two shots, special efforts were made to remove this possible problem and the maximum angles returned to their usual lower values. Hence, the data from these two shots were not used when the power law fits shown in figure 3 were constructed. Also, the maximum angles for the copper hemisphere shot were much larger than those for any other shots at comparable pressures. Further, the vertical swerve for this shot was much different than those for previous and later shots. (Swerves will be discussed at a later point.) Hence, this was regarded as a poor-quality launch shot and was also excluded when the power law fits shown in figure 3 were made. Because the maximum angles for the two types of projectiles in the pressure range 380–440 Torr were very similar, the data for the two types of projectiles were grouped together to make the power law fits shown in figure 3.

Because the wavelength data for the two different types of projectiles in figure 4 were significantly different in the pressure range of 380–440 Torr, different fits were made for each type of projectile. None of the data of table 1 was excluded when these fits were made, except for the single data point for the copper hemisphere projectile.

In figures 3 and 4, the data sets are small enough and there is enough data scatter that a one-parameter power law curve with the theoretical exponent of -0.5 can be used to the fit the data within the rms standard-deviation scatter band of a two-parameter power law. In other words, the data scatter does not allow one to distinguish between the free-fit exponents (-0.61, -0.54, and -0.71) and the theoretical exponent of -0.5. A substantially larger quantity of data would be required to establish statistically that the experimental data trends did not follow the theoretical (range pressure)$^{-0.5}$ predictions. Twelve of the fourteen oscillation wavelength data points for the hemisphere-nose projectiles are below the scatter band for the 70-degree sphere-cone projectiles. This likely reflects a significant stability difference between the two projectile designs of different shapes.

The experimental data points are much more closely grouped around the fit lines for the oscillation wavelengths than for the maximum pitch/yaw angles. (Note that the ratio of the maximum to minimum ordinates is the same in figures 3 and 4.) This can be explained as follows. There is a large random component of the initial pitch and yaw rates impressed on the projectile as it passes through the turbulent muzzle-blast region. These random pitch and yaw rates produce directly corresponding maximum pitch and yaw angles for a given projectile. However, for angles that are not too large, for a given projectile and gas density in hypersonic flow, the angular restoring moment varies nearly linearly with the pitch and yaw angles. Hence, the angular oscillations of the projectile are a reasonably good approximation to simple harmonic motion and the frequency of these oscillations does not depend, to first order, upon their amplitude. This leads directly to the conclusion that the wavelength of the pitch and yaw oscillations does not depend upon their amplitude and hence on the large random component of the initial pitch and yaw rates. Thus, the large random components of the initial pitch and yaw rates produce directly corresponding random components on the maximum

pitch and yaw angles but have almost no effect on the oscillation wavelengths. Hence, the relatively large scatter apparent in figure 3 and the much smaller scatter seen in figure 4.

Figures 5 and 6 show the vertical and horizontal swerves of the projectiles for shots 2319–2332. (Swerves are the distances of the projectile from the range centerline.) Swerves are very important because swerve values greater than 5–6 cm can place some or all of the projectile outside the field of view of the cameras. Most of the swerve data were taken at shadowgraph station 13. (The Ames Aerodynamics Range has 16 equally spaced orthogonal shadowgraph stations at intervals of 1.52 m.) Station 13 is the most downrange station available for shadowgraphs when an ICCD camera is used to take head-on images at station 15, as in the present study. When the shadowgraphs at station 13 were unreadable or non-existent, swerves were measured at stations 11 or 12. Vertical swerves were measured at station 12 for shots 2319, 2321, 2322, and 2332. Horizontal swerve was measured at station 11 for shot 2327. The gun was found to shoot about 2.5 cm below range centerline on the average with a scatter range of ±1.5 cm, except for shot 2327 (fig. 5). The gun was found to shoot about 2.5 cm south of the range centerline on the average with a scatter range of ±3 cm (fig. 6). For 12 of the 14 shots for which data are shown in figures 5 and 6, the swerves at shadowgraph stations 7 and 15 were sufficiently small to keep the projectiles completely within the field of view of the ICCD cameras at these stations. For shot 2327, about 15% of the projectile image was lost at station 15. (The projectile was too high.) For shot 2331, about 25% and 50% of the projectile images were lost at stations 7 and 15, respectively. (The projectile was too far to the south of the range centerline.) For shot 2332, the center of the camera view field was moved about 2.5 cm south of range center to allow for the tendency of the gun to shoot south of range center. Full ICCD camera images were obtained in shot 2332. Figure 5 shows that the vertical swerve for the hemispherical copper head projectile is very different from the swerves for earlier or later shots, as mentioned before.

V. SURFACE TEMPERATURE MEASUREMENT TECHNIQUE

Use of Helium in the Ballistic Range

The surface temperatures of the graphite-nose projectiles were determined by measuring the thermal radiation from the graphite surface. While flying through air in the range, the projectile nose is surrounded by a cap of very hot radiating gas (i.e., the shock layer), which adds to the radiation from the graphite surface. Hence, the radiating gas cap must be stripped away when the ICCD camera photographs are taken to allow accurate determination of the graphite surface temperature. This has been done by passing the projectile through small regions where most of the air in the range has been replaced by helium. In our current setup, the projectile flies through ~19 m of air, then through ~20 cm of helium (where the first ICCD camera picture is taken), then through ~12 m more of air, and finally through ~20 cm more of helium (where the second photograph is taken).

At the Ames Aerodynamics Range, we have used both helium chambers and chimneys to produce free helium plumes and to provide nearly air-free regions in which to take ICCD camera images. An earlier helium chamber and earlier helium chimneys were described in reference 17. Here, we describe only the latest and most effective helium chimney, shown in figure 7. Helium is introduced

into the bottom of the chimney, which has a diameter of ~20 cm and a height of ~30 cm. The helium passes through two hole plates, furnace filter material, and finally through a 100 mesh wire screen to produce nearly uniform flow at the exit of the chimney. The lower hole plate has a low flow resistance, with 0.315-cm-diameter holes and a 30% open area. The upper hole plate has a high flow resistance, with 0.168-cm-diameter holes and a 13% open area. The 100 mesh screen (100 openings per inch) has a 36% open area. Two of these chimneys were built.

When the helium chimney was tested at 1 atm pressure, it was operated at a flow rate of 198 standard liters/sec of helium, giving a plume exit velocity of 6.1 m/sec. Under lower-pressure operating conditions in the ballistic range, the flow rate through the chimney was reduced in proportion to the range pressure in atmospheres. Under the 1-atm test conditions, air concentration measurements were made 16.5 cm above the chimney exit. At distances of 7.6 and 8.9 cm from the chimney centerline, the air concentrations were measured to be 3% and 10%, respectively. (These measurements were made with an oxygen deficiency meter, which was also checked with a pure helium flow.) This chimney should, then, provide a cylindrical region ~15 cm in diameter and ~16.5 cm high with air concentrations less than 3% and a cylindrical region ~18 cm in diameter and ~16.5 cm high with air concentrations less than 10%. The ICCD camera images are taken when the projectile is in these low-air concentration regions. The helium flow to the chimneys is turned on about 3 seconds before the shot. The helium flows upwards across the range and then spreads out on the range ceiling on account of its very low density. The helium flow thus does not affect the gas composition in the range except within the actual helium plumes.

Detailed radiation calculations were made for a flight velocity of 4.5 km/sec at 1 atm and at 0.1 atm pressure. Calculations were done for air and for a mixture of 15% air and 85% helium. The calculations were done by J. Olejniczak (ref. 20) using the NEQAIR code (ref. 21). The gas-cap radiation was calculated to be reduced by 5–6 orders of magnitude in the helium/air mixture and to be 1–2 orders of magnitude less than that from a black body at 750 K over the range of wavelength sensitivity of the ICCD cameras. This temperature is the lowest temperature at which the ICCD cameras can detect radiation from a black-body surface.

The gas-cap radiation levels in the helium plumes were verified experimentally by firing a copper hemisphere-nose model through the helium plumes. Because of the high thermal conductivity of copper, the copper surface temperature will be much lower than that of a graphite-nose projectile, and the thermal radiation from the copper will be too weak to detect with the ICCD cameras. Thus, if the gas-cap radiation is removed in the helium plumes, the images of the copper-nosed projectile should appear dark. A copper hemisphere-nose projectile was fired into 380-Torr air in shot 2327. The muzzle velocity was 4.71 km/sec, and the ICCD images were taken in the plumes of the two helium chimneys at velocities of 4.39 and 4.22 km/sec. No gas-cap radiation was detected in either image. Tests under nearly identical conditions performed earlier, but without the helium plumes, showed very strong gas-cap radiation in 100% air.

Expulsion of Graphite Debris from the Projectile Surface

The graphite noses of the projectiles were prepared in two different ways. Many of the earlier graphite-nose projectiles launched in the present program were pre-ablated in one of the ARC arcjets to provide known surface roughnesses. Several images of this class of projectile were presented in

reference 17. An image from a more recent launch of a pre-ablated projectile is shown in figure 8a. Since it is difficult, expensive, and time-consuming to perform arcjet ablation of the graphite projectile noses, we developed a technique where the projectile noses are machined and then bead-blasted to provide a known roughness. The images from the first few bead-blasted projectiles showed a large, anomalous amount of radiation in the nominally laminar flow zone, plus many streaks radiating outwards from the projectile nose. These features were not present in images taken from the arcjet-ablated projectiles and were severe enough to partially obscure the images and to prevent useful surface temperature data from being obtained. A typical image of this type is shown in figure 8b.

It is believed that the problem is caused by fine graphite dust that is a residue of the machining and bead-blasting operations. This dust then remains embedded between the asperities of the graphite surface and cannot be removed by simply cleaning the surface with a jet of dry nitrogen. However, the dust may be shaken loose by the shock waves that pass through the projectile in the launch process. Further, the porous graphite will be pressurized to 50–150 atm by the ram pressure produced during flight though the air down the range. Upon entering the helium plumes, the ram pressure reduces by a factor of ~6, which could permit a strong air flow out of the graphite, carrying graphite dust particles with it.

Liquid-bath ultrasonic cleaning was considered to remove the graphite dust, but rejected because of the risk that the liquid used could compromise the strength of the epoxy or the Nylon used in the construction of the projectile. Further, if any liquid remained absorbed in the graphite, this could lead to steam or vapor explosions in the graphite when heated in flight.

A nitrogen-flow "ultrasonic" cleaning process was developed to clean the graphite surface. Two sectional views of this device are shown in figure 9. This device consists of a 2.5-cm-diameter chamber 2.5 cm high, with a dry nitrogen jet coming into the side of the chamber through a 0.46-cm inside-diameter tube, as shown in the figure. The jet passes over the end of a 0.64-cm-diameter hole containing a tuning slug, exciting strong pressure oscillations. The projectile is held, inverted, just above the oscillation device, as shown. Typically, peak-to-peak oscillation amplitudes of ~0.10 atm are obtained at ~17 kHz frequency at a nitrogen flow rate of ~9 standard liter/sec. The projectile is typically subjected to five periods of 30 seconds of oscillations at 5-minute intervals. The waiting periods are to avoid excessive cooling of the nitrogen gas in the cylinder and possible water condensation from room air on the projectile.

Figure 8c shows an ICCD camera image of a projectile that was bead-blasted and then cleaned with the new oscillating nitrogen-flow cleaning device. The anomalous radiation in the laminar flow region and the streaks seen in figure 8b are absent, and the radiation levels (when properly scaled) are very close to those observed in the image of the arcjet-ablated projectile shown in figure 8a. Thus, the nitrogen-flow cleaning device is apparently effective at eliminating the graphite dust problem. (Note that all three projectile images shown in figure 8 were taken at nearly identical range pressures and projectile velocities.)

Cameras Used to Photograph Projectiles, Range Optical Setup

The projectiles were photographed using two Roper Scientific PI.MAX:512HQ (ref. 14) ICCD cameras. These cameras have a 512 x 512 imaging array and a wavelength sensitivity of roughly 480 to 900 nm. Exposure times of 1 microsec were used in order to "freeze" the motion of the projectile. The projectiles were viewed from angles of 10–15 degrees away from head-on, using expendable first-surface mirrors. These cameras were set up to photograph the projectile just downstream of shadowgraph stations 7 and 15. An Indigo Phoenix (ref. 15) mid-infrared (IR) camera with a 320 x 256 imaging array, a wavelength sensitivity of 1.5–5.0 microns, and a minimum exposure time of 0.5 microsec was used for temperatures lower than those detectable using the ICCD cameras. The ICCD cameras used Nikon Nikkor 180-mm f/2.8 lenses at f/8 and a B and W 090 long pass filter with a cut-off of ~530 nm. The IR camera used a Janos Technology Asio series 100-mm f/2.3 lens (3–5 micron), a 3–5 micron band-pass filter, and an IR neutral density filter. (Densities of 2 or 3 were used, depending upon the shot.) With the IR camera, a 15-cm-diameter clear-aperture silicon window is used in the range so that the full wavelength range of the camera can be used. This camera also viewed the projectiles nearly head-on, using expendable mirrors. It was set up to take photographs at shadowgraph station 3 in the ballistic range.

The Roper Scientific cameras were calibrated using a black-body furnace source that can reach temperatures up to 1470 K. (For higher-temperature calibrations, a second black-body furnace source is available that can reach temperatures up to 3270 K.) The optical system used during the calibrations was set up the same way as the optical system used to take data in the range. The emissivity of the POCO graphite in the temperature range of interest is roughly 0.8. The cameras had maximum counts/pixel of 65,535 (16 bit) and typical dark noise levels of ~100 counts/pixel. Between 1200 and 1470 K in the calibration, the uncertainty in the temperature ranged from 2 to 7 K. For lower temperatures, the uncertainty is higher, but as long as the camera signal is greater than ~2% of full scale, the uncertainty in temperature is less than 10 K. These uncertainties were determined experimentally, based on noise levels, during the furnace calibrations.

The optical setup in the range for the ICCD camera at shadowgraph station 7 is shown in figure 10. (The muzzle-blast dump tank is located between the gun muzzle and shadowgraph station 1, but it is not shown in the figure.) The projectile is shown at two different times in its trajectory. When the projectile passes through the light beam at station 7, a pulse is produced in the photocell output. This pulse is then delayed through a timer unit so that the image is taken when the projectile is in the center of the plume from the helium chimney. An nearly identical setup is used at station 15 to take a second ICCD camera image. For the IR camera, no helium plume is used and the image is taken directly at station 3, rather than ~60 cm downrange of the triggering station, as shown in figure 10. (At the IR wavelengths, the gas-cap radiation is extremely low compared to the radiation from the graphite surface.) The view shown in figure 10 is from the side of the range. The light beam and helium chimney are shown as they actually are, but the optical path for the camera is shown rotated into the vertical plane in the interest of clarity; it is actually in the horizontal plane.

VI. ICCD AND IR IMAGES OF PROJECTILES, PRELIMINARY TEMPERATURE FIELD DATA

Figure 11a shows an ICCD camera image of a hemisphere-nose graphite-nose projectile taken in the helium plume ~60 cm downrange of shadowgraph station 15. The projectile was flying at 4.50 km/sec in 190-Torr air. Figure 11b shows an ICCD camera image of a 70-degree sphere-cone graphite-nose projectile taken in the helium plume ~60 cm downrange of shadowgraph station 7. The projectile was flying at 4.01 km/sec in 571-Torr air. (All projectiles discussed in this section were bead-blasted and ultrasonically cleaned in the nitrogen flow device described in section V. The roughness produced by the bead blasting will be quantified at a later time by microscopic examination.) The dark regions in the center of each photograph are the laminar-flow regions, where the heat transfer rates and hence, the graphite temperatures, are lower. Outside of the laminar-flow region is the transition region, where the flow changes from laminar to turbulent. The bright annulus outside of the laminar-flow region is the turbulent-flow region, where the heat transfer rates and graphite temperatures are higher than in the laminar-flow region. The seven or eight fiducial holes are visible outside of or at the edge of the bright turbulent-flow region.

Figure 12 shows an IR camera image of a graphite hemisphere-nose projectile taken at shadowgraph station 3. The projectile was flying at 4.65 km/sec in 190-Torr air. This picture was taken through a neutral density #2 filter. At this station, the projectile was only 13.1 m from the gun muzzle, compared to 19.8 and 32.0 m for shadowgraph stations 7 and 15, respectively, where the ICCD camera images were taken. Hence, the temperatures of the graphite surface were lower at station 3 than at stations 7 and 15. Figure 13 shows a preliminary normalized surface temperature field obtained from the ICCD image shown in figure 11b. This temperature field was obtained from the raw ICCD camera image data of figure 11b and is normalized with respect to the stagnation point temperature.

We note here that all of the projectiles shown in figures 11–13 were launched with muzzle velocities of 4.70–4.75 km/sec. The differing velocities of the projectiles noted above were due to the different range pressures, different drag coefficients, and different stations at which the images were obtained.

The ICCD camera and IR camera data are currently being analyzed to obtain correlations of transition data. Analyses are also in progress to obtain final graphite surface temperature data and final heat transfer data.

VII. SUMMARY AND CONCLUSIONS

A research effort to advance techniques for determining transition location and measuring surface temperatures on graphite-tipped projectiles in hypersonic flight in a ballistic range was described. Projectile design and launcher operating conditions were discussed. The projectiles launched to date were bore-rider, free-flying hemisphere-nose and 70-degree sphere-cone projectiles. Three different plastics (ABS, polyethylene, and Zytel ST 801 Nylon) were tested for the projectile afterbodies.

Based upon density, strength, and burning and smoking properties, Nylon became the plastic of choice.

The operating conditions for the Ames 3.81-cm light gas gun needed to obtain the desired launch conditions (projectile masses of 96–115 g; muzzle velocities of 4.6–5.1 km/sec) were given. Because the projectiles were free-flying, it was necessary to minimize their maximum pitch and yaw angles. Most of the projectiles launched to date had maximum angles of 3–6 degrees for range pressures of 190–380 Torr and maximum angles of 2.5–5 degrees for range pressures of 380–570 Torr. The maximum pitch and yaw angles and the projectile oscillation wavelength were found to vary as the range pressure to the -0.5 power, as predicted theoretically.

A helium chimney plume system used to remove the radiating gas cap around the projectile at the location where the ICCD camera pictures were taken was described. This system provided a cylindrical region ~15 cm in diameter and ~16.5 cm high with air concentrations less than 3%. The performance of the helium plumes was verified by firing a copper hemisphere-nose projectile at a muzzle velocity of ~4.7 km/sec into 380-Torr air in the range. ICCD camera images were obtained in the two helium plumes; no gas-cap radiation could be detected in either image.

Bead-blasted projectiles were found to retain fine graphite dust as a residue of the machining and bead-blasting operations. This dust apparently became embedded in the graphite surface, but can be released during flight down the ballistic range, particularly within the helium plumes, obscuring the surface of the projectile. A nitrogen-flow "ultrasonic" cleaning process was developed to clean the graphite surface. Oscillation amplitudes (peak-to-peak) of ~0.10 atm at ~17 kHz frequency are produced by a nitrogen jet in a small chamber. The projectile nose is placed just outside the chamber exit. Cleaning the graphite surface for ~2.5 minutes in this way has allowed us to obtain high-quality images of the projectiles.

Finally, a number of ICCD and infrared camera images of hemisphere-nose and 70 sphere-cone projectiles at velocities of 4–4.7 km/sec and range pressures of 190–570 Torr were presented. Transition from laminar to turbulent flow is clearly visible in these images. Preliminary normalized surface temperature data are shown for a 70-degree sphere-cone projectile.

REFERENCES

1. Reda, D. C.: Review and Synthesis of Roughness-Dominated Transition Correlations for Reentry Applications. Journal of Spacecraft and Rockets, vol. 39, no. 2, March-April 2002, pp. 161–167.

2. Reda, D. C.: Correlation of Nosetip Boundary-Layer Transition Data Measured in Ballistic-Range Experiments. AIAA Journal, vol. 19, no. 3, March 1981, pp. 329–339.

3. Reda, D. C.; Leverance, R. A.; and Longas, S. A.: Aerothermodynamic Testing and Analysis of Reentry Vehicle Nosetips in Hypersonics Ballistics-Range Flight. 22nd International Instrumentation Symposium, Instrument Society of America, San Diego, CA, May 1976.

4. Reda, D. C.; and Leverance, R. A.: Boundary-Layer Transition Experiments on Pre-Ablated Graphite Nosetips in a Hyperballistics Range. AIAA Journal, vol. 15, March 1977, pp. 305–306.

5. Reda, D. C.; and Brown, H. S.: Analysis of Nosetip Boundary-Layer Transition Data Using Interactive Graphics. 24th International Instrumentation Symposium, Instrument Society of America, Albuquerque, NM, May 1978.

6. Reda, D. C.; and Raper, R. M.: Measurements of Transition-Front Asymmetries on Ablating Graphite Nosetips in Hypersonic Flight. AIAA Journal, vol. 17, November 1979, pp. 1201–1207.

7. Reda, D. C.: Comparative Transition Performance of Several Nosetip Materials as Defined by Ballistics-Range Testing. 25th International Instrumentation Symposium, Instrument Society of America, Anaheim, CA, May 1979; also, ISA Transactions, vol. 19, no. 1, 1980, pp. 83–98.

8. Norfleet, G. D.; Hendrix, R. E.; and Jackson, D.: Development of a Hypervelocity Track Facility at AEDC. AIAA Paper 77-151, 15th Aerospace Sciences Meeting, Los Angeles, CA, January 1977.

9. Anderson, A. D.: Passive Nosetip Technology (PANT) Program. Interim Report, volume X, App. A: Boundary Layer Transition on Nosetips with Rough Surfaces. SAMSO-TR-74-86, January 1975.

10. Dirling, R. B., Jr.; Swain, C. E.; and Stokes, T. R.: The Effect of Transition and Boundary Layer Development on Hypersonic Reentry Shape Change. AIAA Paper 75-673, 10th Thermophysics Conference, Denver, CO, May 1975.

11. van Driest, E. R.: Evaluation of PANT Transition Roughness Data and Transition Criterion. Unpublished memo to SAMSO, November 1975.

12. Finson, M. L.: An Analysis of Nosetip Boundary Layer Transition Data. AFOSR-TR-76-1106, August 1976.

13. Bishop, W. M.: Transition Induced by Distributed Roughness on Blunt Bodies in Supersonic Flow. AIAA Paper 77-124, 15th Aerospace Sciences Meeting, Los Angeles, CA, January 1977.

14. User Manual 4411-0069, Version 2.A, October 18, 1999, PI-MAX Camera (Princeton Instruments), Roper Scientific, 3660 Quakerbridge Road, Trenton, NJ, 08619.

15. Technical information on Phoenix cameras from Indigo Systems Corporation. 50 Castilian, Goleta, CA, 93117.

16. Bogdanoff, D. W.; and Reda, D. C: Technique for Transition Measurements on Hemisphere Nose Projectiles at Hypersonic Velocities—Projectile Design and Launcher Issues. Presented at the 53rd Meeting of the Aeroballistic Range Association, Sendai, Japan, October 21–25, 2002.

17. Bogdanoff, D. W.; and Wilder, M. C.: Technique for Transition and Heat Flux Measurements on Projectiles at Hypersonic Velocities. Presented at the 54th Meeting of the Aeroballistic Range Association, Santa Fe and Albuquerque, NM, USA, October 19–24, 2003.

18. Brochure E-71043 from E. I. duPont de Nemours and Co., Polymer Products Division, Wilmington, DE 19898, USA.

19. Anderson, J. D., Jr.; Hypersonic and High Temperature Gas Dynamics. McGraw-Hill, New York, 1989, p. 262.

20. Olejniczak, J.: Private communication, 2003.

21. Whiting, E. E.; Park, C.; Liu, Y; Arnold, J. O.; and Paterson, J. A.: NEQAIR96, Nonequilibrium and Equilibrium Radiative Transport and Spectra Program: User's Manual. NASA Reference Publication 1389, December 1996.

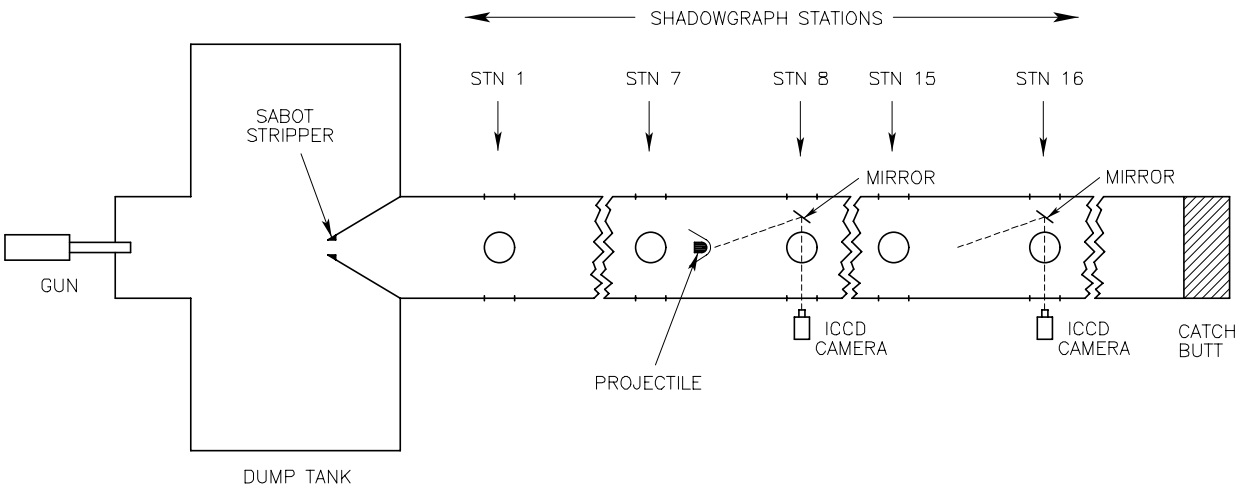

Figure 1. Ames Aerodynamics Range.

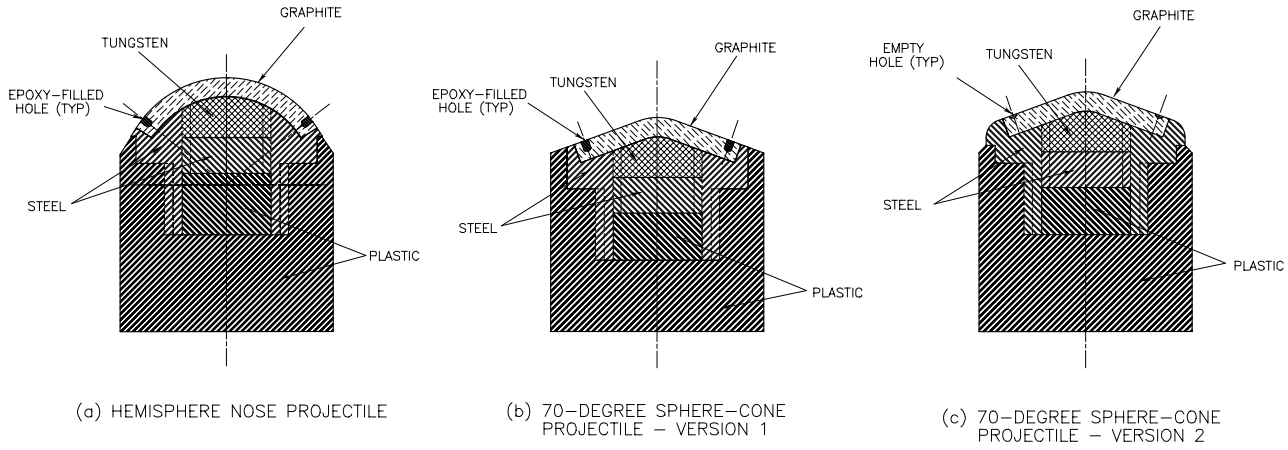

Figure 2. Projectiles launched in the present study.

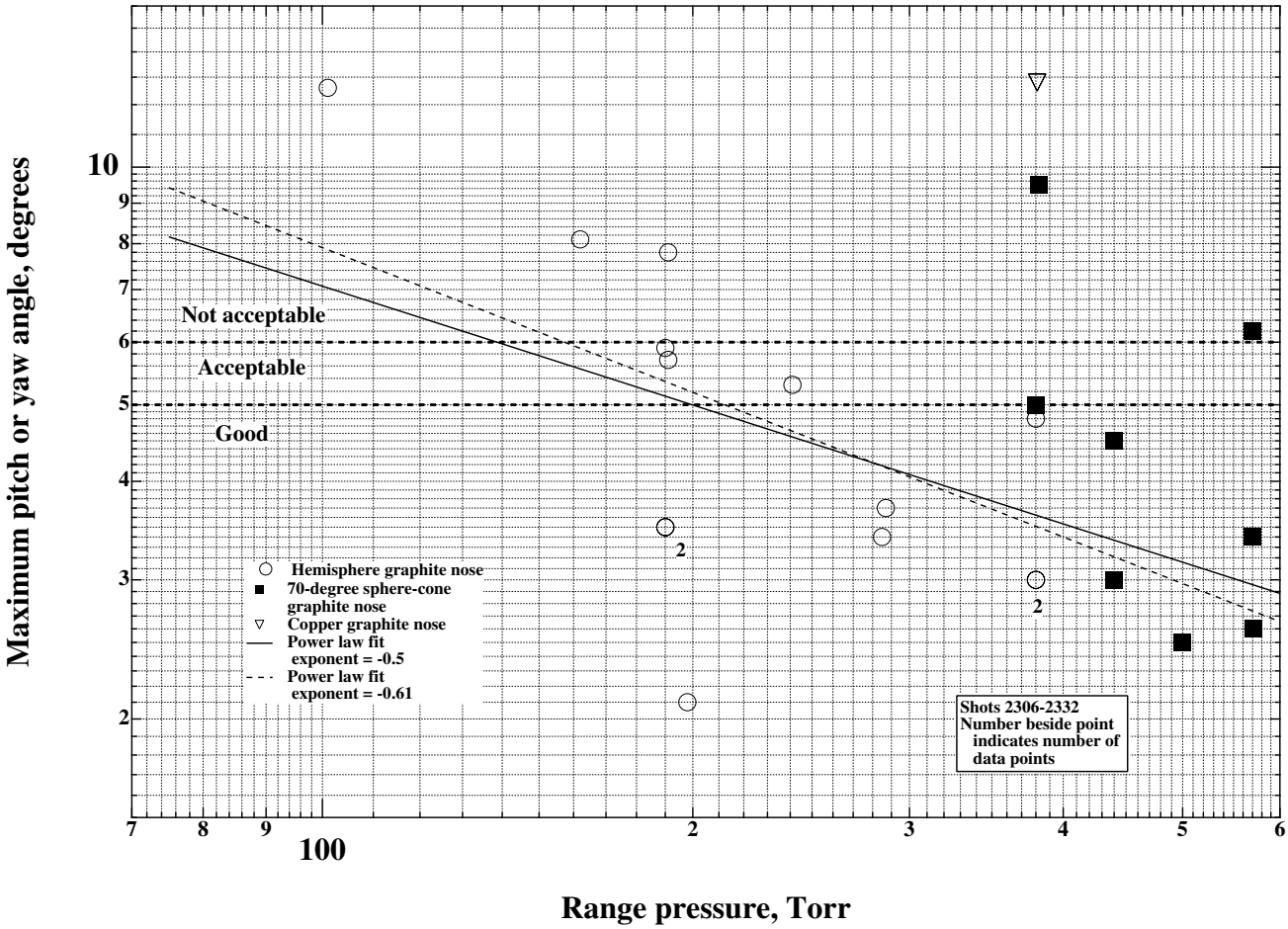

Figure 3. Maximum pitch or yaw angle vs. range pressure.

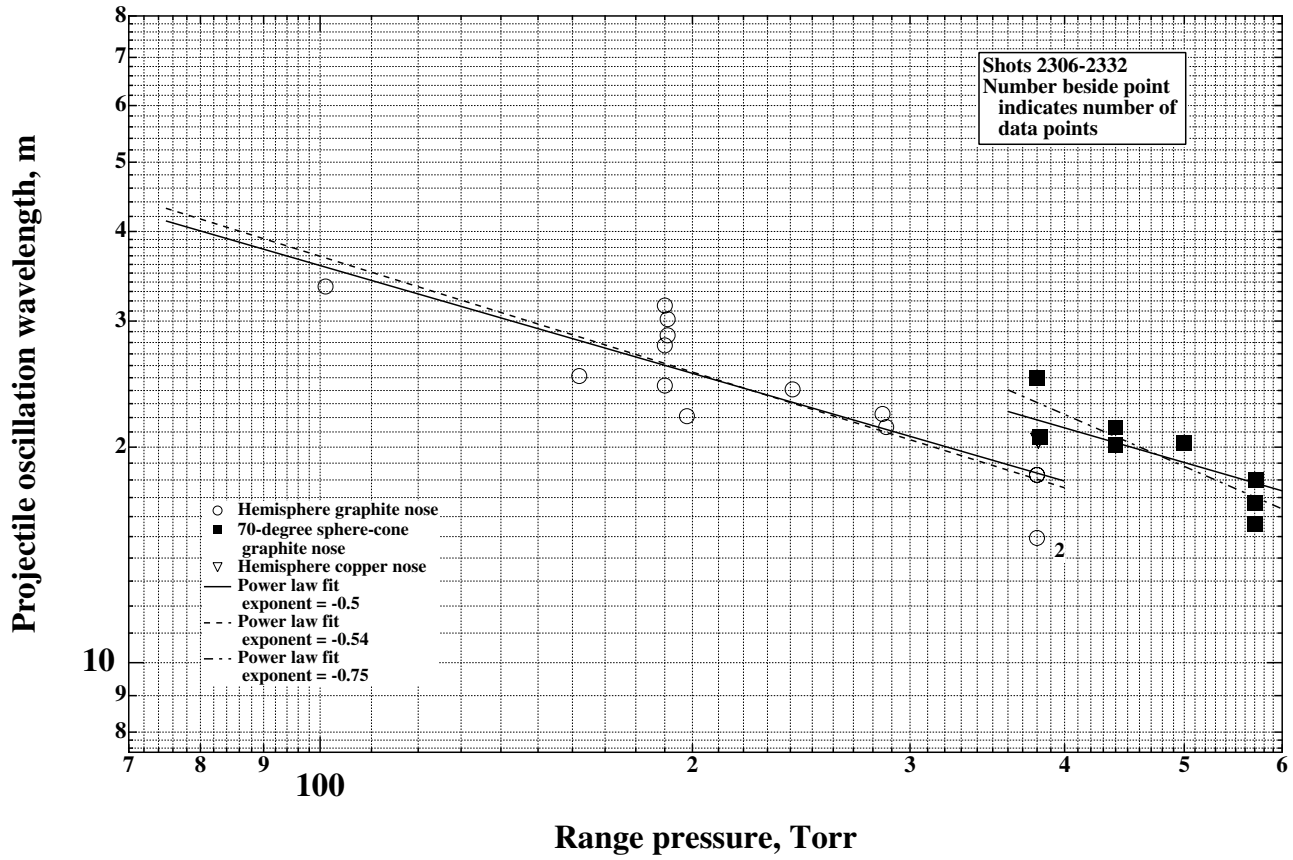

Figure 4. Oscillation wavelength of graphite-nose projectiles vs. range pressure.

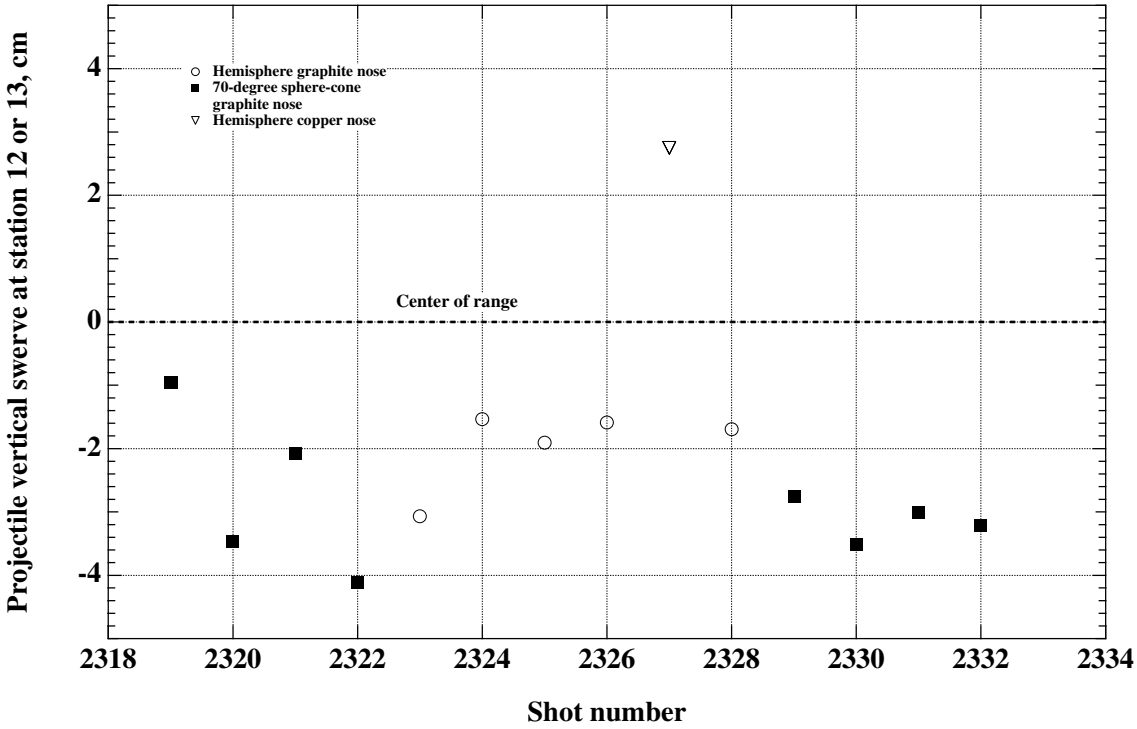

Figure 5. Projectile vertical swerve vs. shot number.

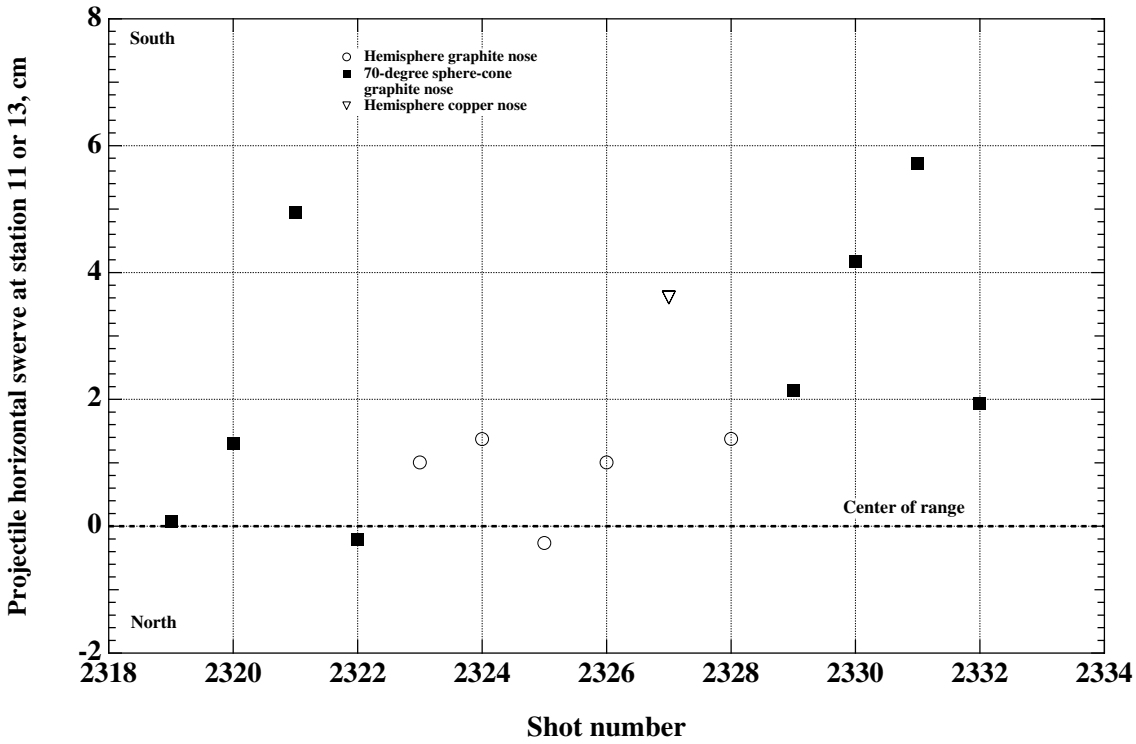

Figure 6. Projectile horizontal swerve vs. shot number.

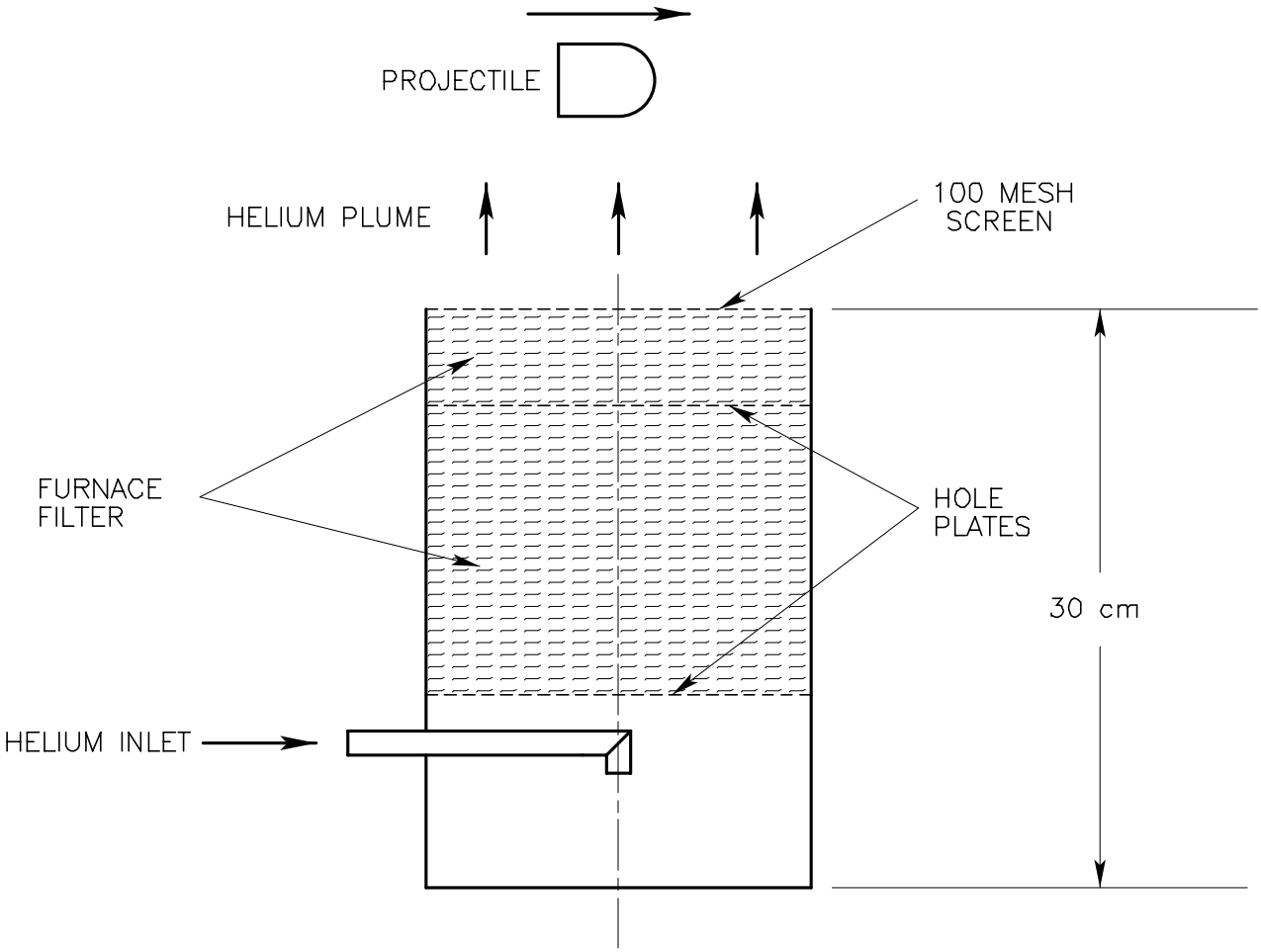

Figure 7. Helium chimney for range.

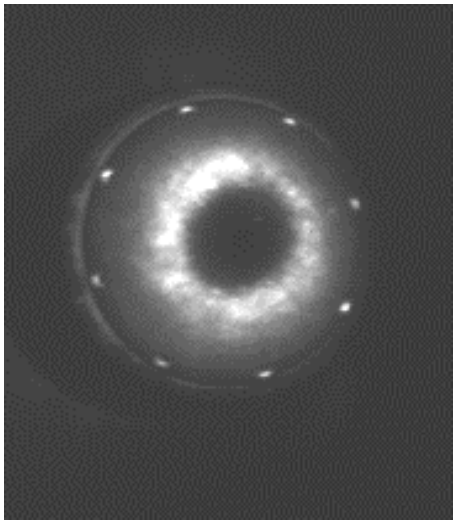

a. Shot number 2326
Range pressure = 191 Torr
Proj. velocity = 4.45 km/sec
Arcjet-ablated surface

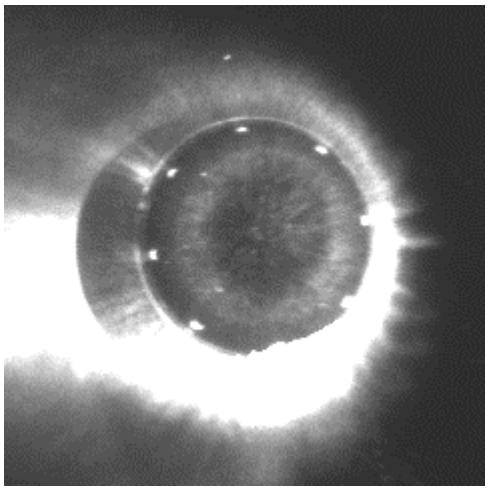

b. Shot number 2324
Range pressure = 190 Torr
Proj. velocity = 4.51 km/sec
Bead-blasted surface

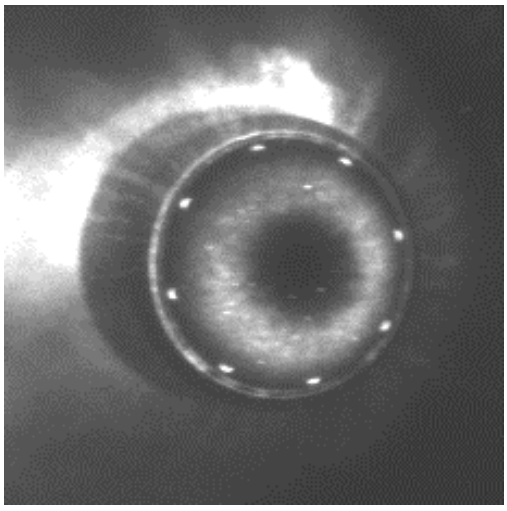

c. Shot number 2328
Range pressure = 190 Torr
Proj. velocity = 4.50 km/sec
Bead-blasted, ultrasonically cleaned surface

Figure 8. ICCD camera pictures of hemisphere-nose projectiles launched into air. All pictures were taken 61 cm downrange of shadowgraph station 15.

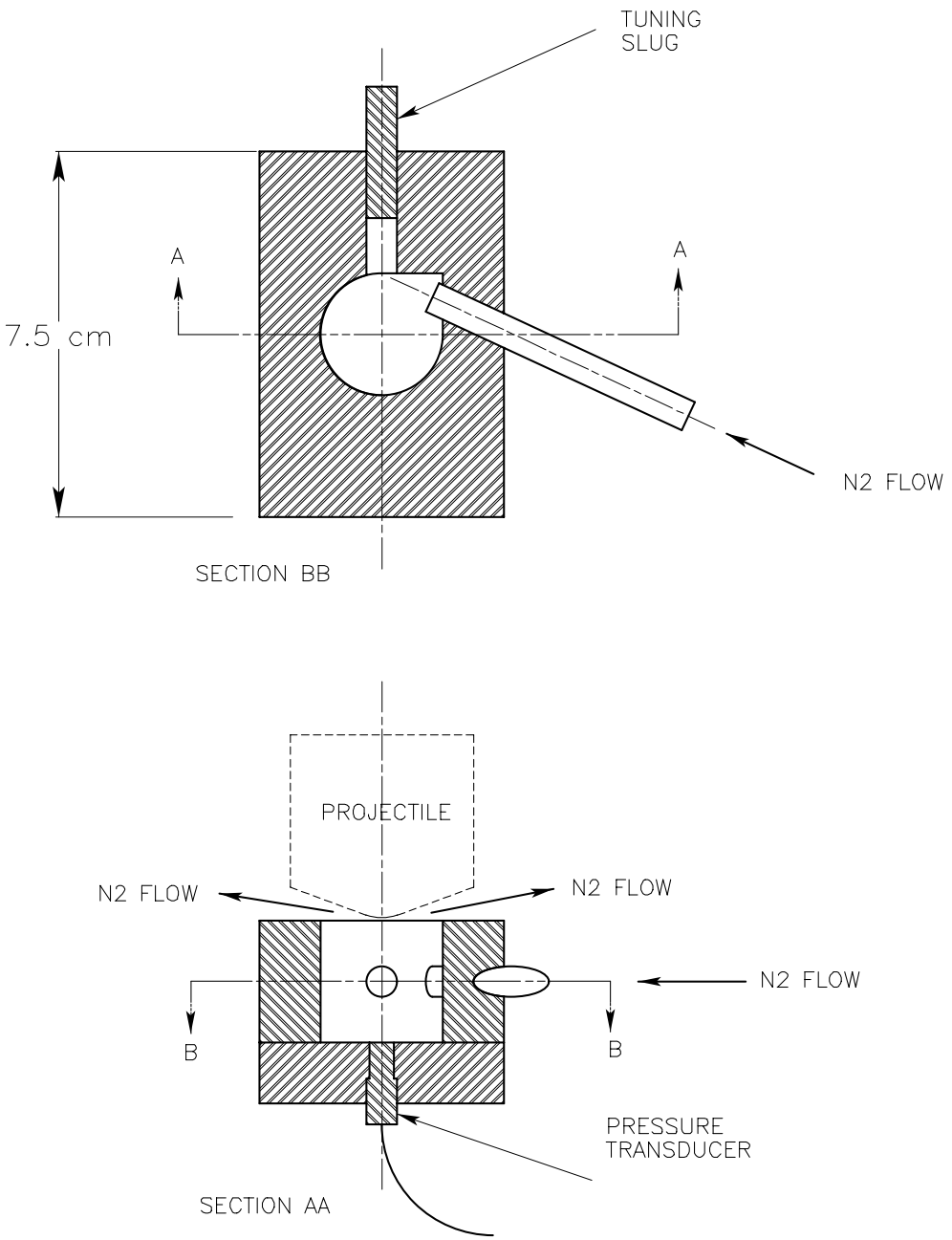

Figure 9. "Ultrasonic" nitrogen flow projectile cleaning device.

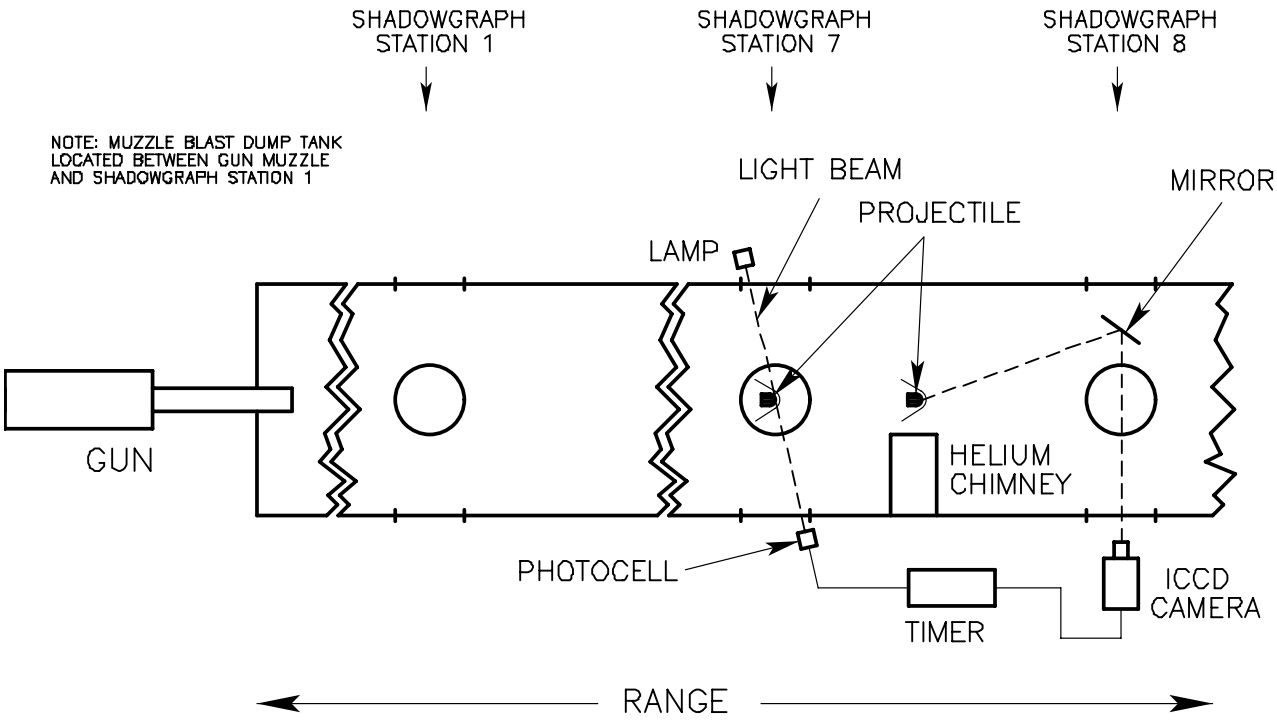

Figure 10. Typical range optical setup.

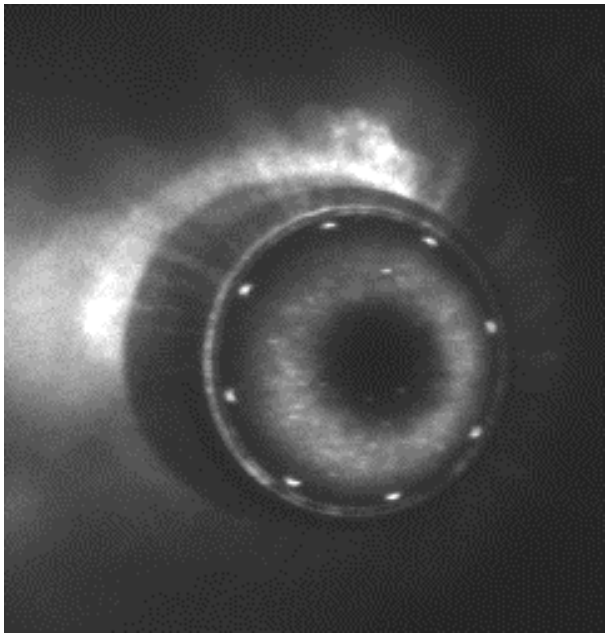

a. Shot number 2328
Range pressure = 190 Torr
Proj. velocity = 4.50 km/sec
$Re_D = 2.80 \times 10^6$
Hemisphere nose
In helium plume at station 15

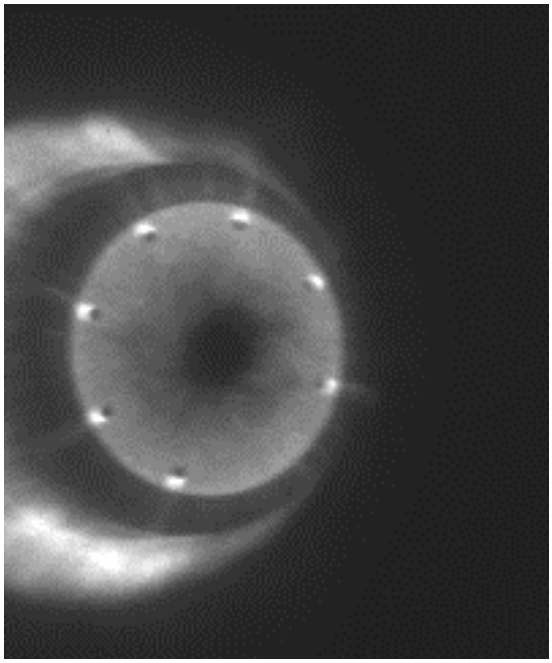

b. Shot number 2329
Range pressure = 571 Torr
Proj. velocity = 4.01 km/sec
$Re_D = 7.49 \times 10^6$
70-degree sphere-cone nose
In helium plume at station 7

Figure 11. ICCD camera pictures of graphite nose projectiles launched into air. Projectiles were bead-blasted and ultrasonically cleaned using the nitrogen flow device shown in figure 8.

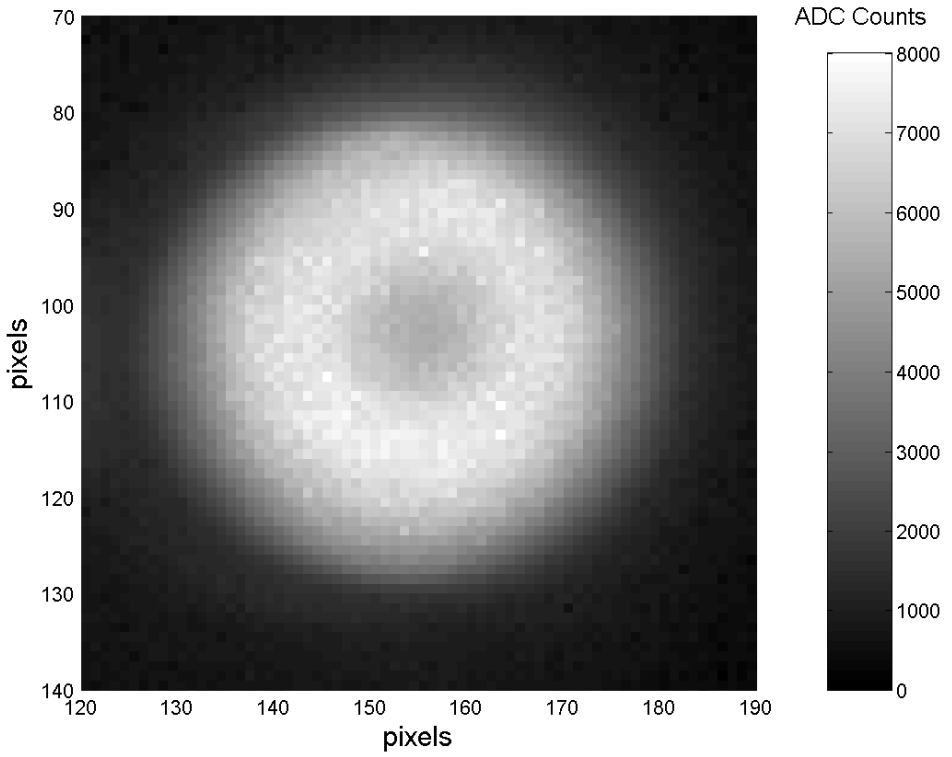

Shot number 2328
Range pressure = 190 Torr
Proj. velocity = 4.65 km/sec
$Re_D = 2.80 \times 10^6$
Hemisphere nose
At station 3

Figure 12. IR camera picture of graphite-nose projectile launched into air. Neutral density #2 filter used. Projectile was bead-blasted and ultrasonically cleaned in nitrogen flow device.

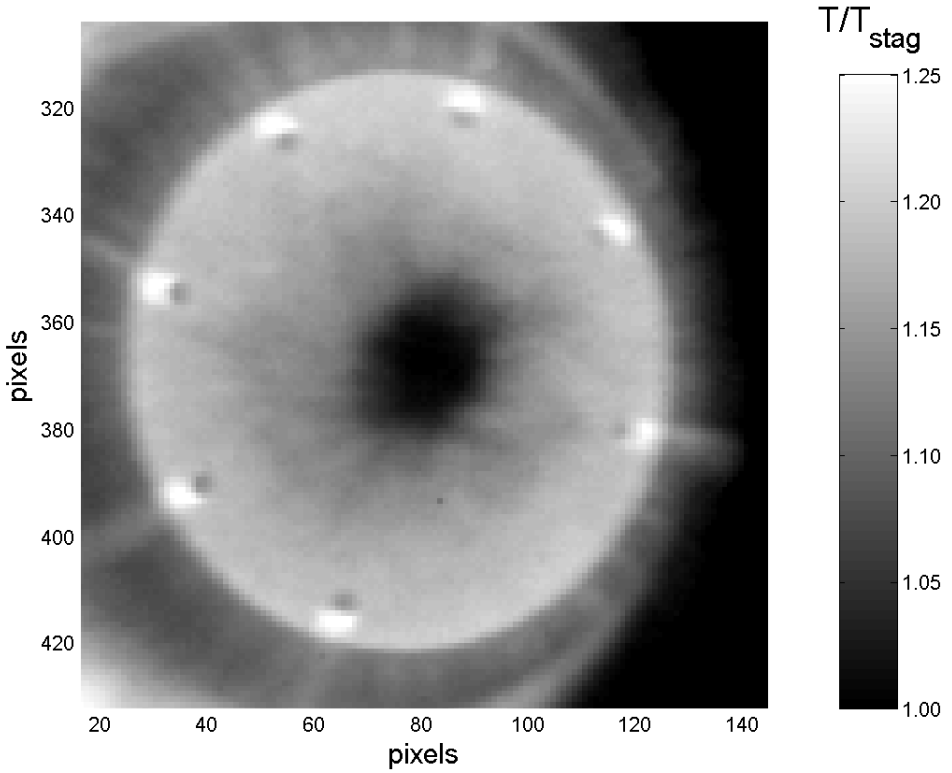

Shot number 2329
Range pressure = 571 Torr
Proj. velocity = 4.01 km/sec
$Re_D = 7.49 \times 10^6$
70-degree sphere-cone nose
In helium plume at station 7

Figure 13. Preliminary surface temperature field for graphite-nose projectile launched into air. Surface temperature in scale to right of image is normalized by stagnation-point temperature. Projectile was bead-blasted and ultrasonically cleaned in nitrogen flow device.

REPORT DOCUMENTATION PAGE

Form Approved
OMB No. 0704-0188

1. REPORT DATE *(DD-MM-YYYY)*	2. REPORT TYPE	3. DATES COVERED *(From - To)*
11/07/2005	Technical Memorandum	

4. TITLE AND SUBTITLE

Techniques for Transition and Surface Temperature Measurements on Projectiles at Hypersonic Velocities—A Status Report

5a. CONTRACT NUMBER

5b. GRANT NUMBER

5c. PROGRAM ELEMENT NUMBER

6. AUTHOR(S)
D. W. Bogdanoff* and M. C. Wilder **

5d. PROJECT NUMBER

5e. TASK NUMBER

5f. WORK UNIT NUMBER
UPN 800-52

7. PERFORMING ORGANIZATION NAME(S) AND ADDRESS(ES)
*ELORET, Sunnyvale, California 94087 and
**Ames Research Center, Moffett Field, CA 94035-1000

8. PERFORMING ORGANIZATION REPORT NUMBER
A-0412610

9. SPONSORING/MONITORING AGENCY NAME(S) AND ADDRESS(ES)
National Aeronautics and Space Administration
Washington, DC 20546-0001

10. SPONSORING/MONITOR'S ACRONYM(S)
NASA

11. SPONSORING/MONITORING REPORT NUMBER
NASA/TM–2005-212831

12. DISTRIBUTION/AVAILABILITY STATEMENT
Unclassified — Unlimited Distribution: Nonstandard
Subject Category 15
Availability: NASA CASI (301) 621-0390

13. SUPPLEMENTARY NOTES
Point of Contact: D. W. Bogdanoff, ELORET, Sunnyvale, California 94087 (650) 604-6138

14. ABSTRACT

A research effort to advance techniques for determining transition location and measuring surface temperatures on graphite-tipped projectiles in hypersonic flight in a ballistic range is described. Projectiles were launched at muzzle velocities of ~4.7 km/sec into air at pressures of 190–570 Torr. Most launches had maximum pitch and yaw angles of 2.5–5 degrees at pressures of 380 Torr and above and 3–6 degrees at pressures of 190–380 Torr. Arcjet-ablated and machined, bead-blasted projectiles were launched; special cleaning techniques had to be developed for the latter class of projectiles. Improved methods of using helium to remove the radiating gas cap around the projectiles at the locations where ICCD (intensified charge coupled device) camera images were taken are described. Two ICCD cameras with a wavelength sensitivity range of 480–870 nm have been used in this program for several years to obtain images. In the last year, a third camera, with a wavelength sensitivity range of 1.5–5 microns [in the infrared (IR)], has been added. ICCD and IR camera images of hemisphere nose and 70 degree sphere-cone nose projectiles at velocities of 4.0–4.7 km/sec are presented. The ICCD images clearly show a region of steep temperature rise indicative of transition from laminar to turbulent flow. Preliminary temperature data for the graphite projectile noses are presented.

15. SUBJECT TERMS
Hypersonic projectiles, Transition, Surface temperatures

16. SECURITY CLASSIFICATION OF:			17. LIMITATION OF ABSTRACT	18. NUMBER OF PAGES	19a. NAME OF RESPONSIBLE PERSON
a. REPORT	b. ABSTRACT	c. THIS PAGE			D. W. Bogdanoff
Unclassified	Unclassified	Unclassified	Unclassified	31	19b. TELEPHONE *(Include area code)* (650) 604-6138